IEEE Access
Multidisciplinary | Rapid Review | Open Access Journal

Received 27 July 2022, accepted 5 August 2022, date of publication 8 August 2022, date of current version 15 August 2022.

Digital Object Identifier 10.1109/ACCESS.2022.3197661

RESEARCH ARTICLE

Optimization of Network-Based Earthquake Early Warning Systems on the Korean Peninsula

SEONGHEUM CHO, JAE-KWANG AHN, AND EUI-HONG HWANG
Earthquake and Volcano Research Division, Korea Meteorological Administration, Seoul 07062, South Korea

Corresponding author: Jae-Kwang Ahn (propjk@korea.kr)

This work was supported by the Development of Earthquake Information Production Technology under Grant KMA2022-02121.

ABSTRACT Most countries and local governments provide earthquake services in the public domain, and they must have high accuracy. If a missed alarm of the Earthquake Early Warning (EEW) system causes many casualties, or if the industrial system is temporarily suspended owing to a false alarm, causing economic losses, it inevitably becomes the responsibility of the government. Therefore, most countries approach the technological improvement of EEW systems carefully by performing simulations and conducting long-term tests to ensure their reliability. In this study, we extract characteristics of the initial P-wave amplitude from an earthquake on the Korean Peninsula and perform trend analysis. We found a common optimal threshold on the Korea Meteorological Administration's seismic observatory network from trend analysis. We then evaluated the performance of the optimized algorithm based on the simulation. The performance evaluated the actual events recorded corresponding to the number of matched, missed, and false events. As the result of the evaluation, the optimized module combination had a significantly lower occurrence of false events than the previous version. Therefore, we expected that the proposed optimization should contribute to improving alarm stability in real-time EEW.

INDEX TERMS Amplitude attenuation, earthquake early warning systems, initial P-wave, quality control, simulation systems.

I. INTRODUCTION

Because natural disasters are areas that humans cannot control, countries spend a significant amount of money on improving their preparedness and response capabilities. For natural disasters, such as heatwaves, heavy snow, and typhoons, the weather is predicted using various observation instruments, such as automatic weather systems, remote sensing, and meteorological radars. This is primarily performed through weather forecasting, and preparation for natural disasters is performed based on accurate forecasts. However, earthquakes, seismic tsunamis, and volcanoes are difficult to predict in a similar manner because their source points are created underground where real-time observation is impossible. Earthquakes are the most difficult disasters to respond to, particularly because vibrations spread rapidly underground. Occasionally, it is implied that earthquakes can be predicted through marvelous phenomena, such as strange behaviors or movements of clouds, insects, and animals. The prediction of earthquake disasters based on such premonitory phenomena is not only weak in scientific evidence, but also inconsistent, causing significant social confusion. Therefore, earthquake alerts can only be generated based on rapid detection.

Earthquake Early Warning (EEW) systems were first conceived by Dr. Cooper in 1868 and are technology that allows for rapid notification prior to S-wave arrivals based on the information of the initial P-wave [1], [2], [3]. In the first step of the EEW system, the core of this technology is to detect P-wave, which can provide time available to mitigate earthquake damage before S-wave or surface wave arrivals.

Seismometers installed to detect earthquakes record 24 h of continuous ground movement and collect both artificial and natural shaking around the seismometer. Large and long-period natural movement can spread great distances, whereas artificial shaking is a temporary and high-frequency component and is not transmitted far. These are called background noise and do not have a large amplitude. In general, the amplitude of the first P-wave in an earthquake is similar to or slightly larger than the background noise level.

The associate editor coordinating the review of this manuscript and approving it for publication was Mauro Gaggero.

Therefore, signal detection in EEW networks is sensitive to background noise, which records movements at the seismometer. However, not all earthquakes signal that the temporary amplitude is slightly larger than the background noise. Therefore, we must determine whether the signal is an earthquake from a small difference.

If a shock signal spreads widely over time, the possibility of an earthquake increases. However, we have focused on the signals recorded at one observatory to determine the speed and accuracy of the EEW system. The detection of impact signals is the first stage of seismic detection, and currently, three methods are used. The first method detects changes in the average amplitude of a waveform, which is the short-term average or long-term average (STA/LTA) or signal-to-noise ratio (SNR) [4], [5]. This is a simple technique for detecting a time point when the amplitude increases owing to the shock wave, compared with the average background noise over an extended period. This method is efficient in detecting signals; however, it is not possible to determine whether the signal corresponds to an earthquake. The second method classifies earthquake and non-earthquake signals through periodic filtering of the detected signals. The filter picker method proposed by Lomax *et al.* [6] empirically detects P-waves based on the waveband of seismic waves. It exhibits a higher level of seismic detection performance than the STA/LTA method [6]. The last is a detection method that utilizes the latest trend in machine learning (ML). Supervised learning has been applied to identify earthquakes in terms of images as changes in seismic signals. Because it is a technology that detects earthquakes through machine learning, it is possible to achieve a higher accuracy than the previous two methods through the composition of learning materials and layer composition [7], [8], [9], [10], [11].

Recently, EEW technologies [11], [12], [13] to which the ML-based picker is applied have been developed and pickings are performed based on the upward slope of the three-component amplitude. At this time, a sufficient time period was required to identify the upward slope of the seismic wave amplitude. However, various problems must be solved to commercialize ML-based EEW technology. First, perfect picking performance cannot be guaranteed [12]. Second, accuracy cannot be guaranteed in an environment that is different from the learning material, and the cause cannot be determined when a false alarm occurs [13]. Therefore, EEW systems are serviced by governments or local governments in the public domain, cannot easily introduce ML-based EEW that contain alarm errors and uncertainties. In particular, false and missed alarms that do not identify the cause can reduce the reliability of the service. For this reason, the Korea Meteorological Administration (KMA) prefers long-term stable technology or/and EEW systems. ElarmS is a globally validated network-based EEW system that applies the STA/LTA detection technique [14]. The STA/LTA method is efficient, but it sensitive to noise. Therefore, we consider all false alarms.

The latest version of ElarmS (E3) includes functions for classifying abnormal signals, such as spikes, S-wave signals, and distant seismic signals, which greatly strengthen the detection capabilities for earthquakes that can cause actual damage alongside technology for reducing false alarms [15]. This technique uses an empirical amplitude and period threshold for P-wave to identify triggers, which is for events within California. Unlike the western United States, on the Korean Peninsula, the soil layer is not deep, and most of the distributed seismometer networks are located 20 or 100 m below the surface [16]. Due to these differences, an optimization step is required when introducing algorithms developed in other regions [17], [18], [19]. Lim *et al.* [20] optimized the filter bank of the E3 and P-wave time window (PTW) for long-distance earthquakes based on earthquake data generated on and around the Korean Peninsula in the past.

In this study, we proposed an optimization method for empirical trigger filters. A regression of initial P-wave properties was performed using past earthquake data recorded in the seismic observation network on the Korean Peninsula, which presents thresholds of empirical trigger filters for regional earthquakes. We also conducted simulation tests using optimized E3 and previous version of ElarmS (E2) to demonstrate the improvement in performance. In order to evaluate the performance of the EEW system in detail, we need to evaluate the performance in terms of source parameter estimation (location, magnitude), accuracy of ground shaking prediction, and lead-time analysis [21]. The evaluation of the performance in this study focuses on only the detection of the initial P-wave without both network density and alerts decision for using station counts. Therefore, we considered the performance of ElarmS for pre-decision-making procedures using a simple evaluation that compares the number of matched, false, and missed events.

II. DATA OF KOREAN PENINSULA EARTHQUAKE

A total of 161 local earthquakes with magnitudes of 2.5 or higher occurred on the Korean Peninsula and in the nearby sea between June 2015 and April 2019. Earthquakes further than 250 km from the Korean seismic networks were excluded. Fig. 1 shows the locations of the earthquakes and seismic stations used. As shown in Fig. 1, the earthquake magnitude was divided into three stages, and expressed by color. Relative magnitudes are expressed in circles.

Fig. 2 shows the P-wave trigger information; 14,987 data points from the earthquake were used for optimization analysis. Trigger information recorded after the P-wave was picked by STA/LTA and used to analyze the initial P-wave amplitude. At this time, the data was manually checked. First, we removed the record data for low-quality sensors. Second, we selected trigger data based on the correlation between travel time and epicenter distance. It excluded the triggered data with a gap from the theoretical P arrival time. Third, non-event signals were removed, which can be visually identified.

In the corresponding earthquake data, aftershocks from the Gyeongju earthquake and those from the Pohang earthquake are largely distributed. Based on these results, the number of earthquakes in 2016 and 2017 is relatively large, and earthquakes with a magnitude of 4.0 or higher are concentrated inland.

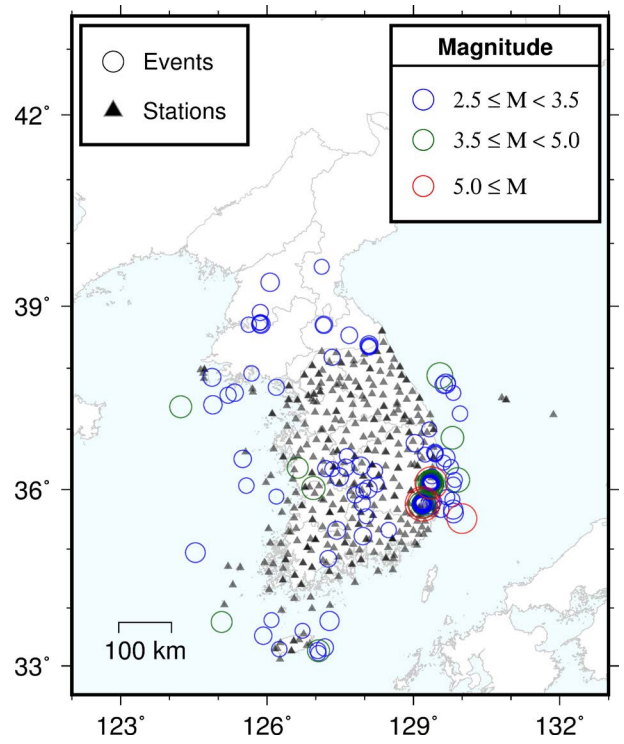

FIGURE 1. Locations of 161 earthquakes and 407 seismic stations on the Korean Peninsula between June 30, 2015 and April 30, 2019.

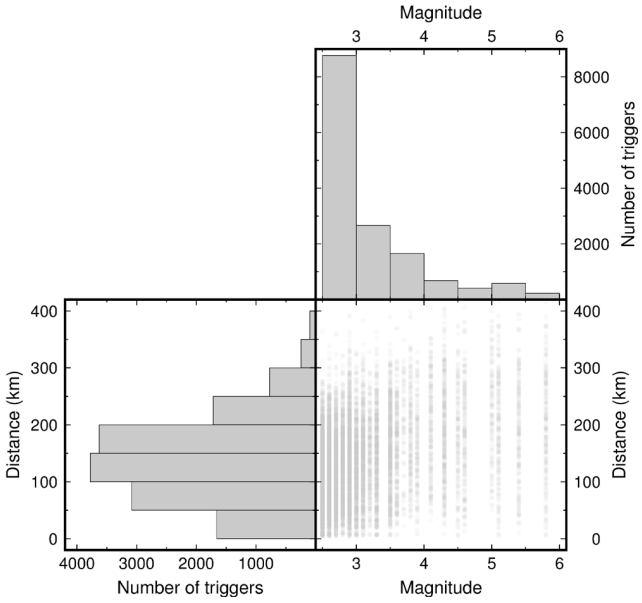

FIGURE 2. P-wave trigger information for 14,987 data points from Korean Peninsula earthquakes.

III. EMPIRICAL FILTER FOR INITIAL P-WAVE

In the network-based EEW algorithm, when the signal is triggered via STA/LTA, it is estimated whether the signal is caused by an earthquake based on the waveform for a period of time in the module. After passing the criteria, it was recognized as a suitable trigger for use in the seismic analysis stage. Therefore, the criteria for the trigger module are the core of EEW for the accuracy of event

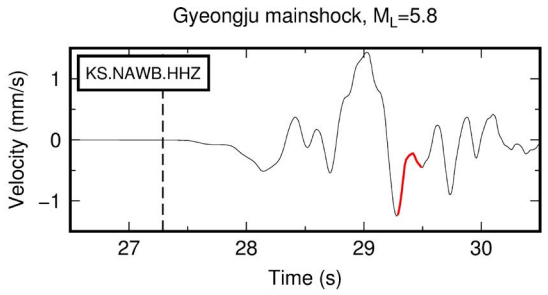

FIGURE 3. Failure case of ZeroCrossing module (ZCM) from a station on September 12, 2016: The red line is the range used to calculate ZCM. M_L 5.8 event was classified as a non-event signal because the waveform did not exceed the zero axis once.

detection. ElarmS-2 (E2) exhibited errors in recognizing signals caused by noise or S-waves as P-wave signals or in analyzing attenuated distant earthquakes as small-scale local events [15]. To resolve these problems, upgraded ElarmS-3 (E3) was added, and the range-post trigger module (RPM), NEtoZ module (NEZM), ZeroCrossing module (ZCM), and teleseismic filter module (TFM) were introduced. Additionally, acceleration and velocity were added to E3, which is the amplitude checks module (ACM) without E2.

ACM performs a simple amplitude test to determine whether the transmitted trigger is a P-wave signal caused by an earthquake. The empirical criteria for the amplitude and period of the initial P-wave vertical component were applied by E3, as summarized in Table 1.

TABLE 1. Criteria for vertical components of the initial P-wave in E3.

Amplitude unit	Criteria
Predominant period(s)	$-0.9 < \log(\tau_p) < 1.0$
Displacement(cm)	$-5.5 < \log(P_d) < 3.5$
Velocity(cm/s)	$-5.5 < \log(P_v) < 3.0$
Acceleration(cm/s^2)	$-2.5 < \log(P_a)$

P_d, P_v, and P_a refer to the maximum displacement, velocity, and acceleration values calculated within the PTW 0.1–0.2 seconds after the trigger, and τ_p refers to the period. The criteria for P_d and τ_p have been used since E2, and the criteria for P_v and P_a were added to E3. The optimization of P_d and τ_p was not considered in this study because these criteria have been used stably in real-time EEW. P_d and epicentral distance are also used in magnitude calculations by applying empirical relationships to the event information calculation process in KMA's EEW [22]. In this study, PTW was used from 0.1–4 seconds after the signal was triggered. Although the accuracy may vary depending on the range of PTW when calculating the magnitude [23], the rising curve of P_d after the trigger converges within 4 seconds even at large magnitude. Therefore, the P-wave amplitude of the trigger used for the initial analysis was a value that passed the minimum criteria, and afterward, the amplitude was updated over time. The seismic information was recalculated based on the updated amplitude.

RTM is used to remove noisy signals, such as boxcars or spikes, the cause of which is unknown [15]. The signal confirms the amplitude change between 0.1 and 0.2 seconds after the trigger, and the calculation formula and criteria are as follows:

$$Vel_{max} - Vel_{min} > 2.2 \times 10^{-6} cm/s \quad (1)$$

$$Acc_{max} - Acc_{min} > 2.2 \times 10^{-3} cm/s^2 \quad (2)$$

where $\mathrm{Vel_{max}}$, $\mathrm{Vel_{min}}$, $\mathrm{Acc_{max}}$, and $\mathrm{Acc_{min}}$ represent the maximum velocity, minimum velocity, maximum acceleration, and minimum acceleration amplitude recorded within 0.1–0.2 seconds after the trigger, and they are calculated as the vector of the three components. If the amplitude change did not exceed the reference value, the corresponding signal was classified as noise and was excluded from the analysis.

NEZM is designed to prevent S-wave signals from being included in seismic analysis and was applied to distinguish S-wave signals by calculating the horizontal to vertical component amplitude ratio (H/V). The principle of NEZM is based on the fact that the amplification effect of P-waves is less than that of S- or Rayleigh waves in the soil layer. H/V is calculated as the ratio of horizontal to vertical components for 0.05 seconds after signal detection, in which case, a component with a larger amplitude among the N (north and south) or E (east and west) components is used as a horizontal component. If H/V exceeds 0.95, it is recognized as an S-wave or noise. The identification expression of the corresponding module is as follows:

$$\frac{H}{V} = \frac{|\max(N) - \min(N)| \, or \, |\max(E) - \min(E)|}{|\max(Z) - \min(Z)|} \leq 0.95 \quad (3)$$

ZCM determines the validity of the signal by counting the number of samples whose amplitudes intersect based on zero (zero-crossing). In the case of single noise or spike-type noise, the number of zero-crossings will be significantly smaller than the actual seismic wave, and thus, the minimum number of zero-crossings is set to identify the P-wave. However, if the P-wave grows longer, ZCM can involve serious errors, which is a problem that occurs mostly in large earthquakes. Fig. 3 presents the waveform of the Gyeongju earthquake, the largest earthquake in Korea, with zero zero-crossings. This suggests that ZCM may be theoretically valid, but has uncertainty in critical earthquakes; thus, it was excluded from the analysis in this study.

IV. SETTING OF SIMULATION FOR PARAMETER ANALYSIS AND VERIFICATION

The open-source software tankplayer of the Linux server-based earthworm [24] was used to simulate the real-time analysis of past earthquakes. To run a tankplayer, multiple miniSEEDs must generate a single file of seismic records called tankfiles. The tankfile is a collection of multiple station records and is applied after reproduction in units of 1-second data packets or samples during the simulation. If the stored tankfile network sends a signal every second, it is similar to an earthquake network delivered in real time. However, problems such as delay time that occur due to the nature of the network are not considered in the simulation; thus, it is reproduced under the condition that the network status is perfect.

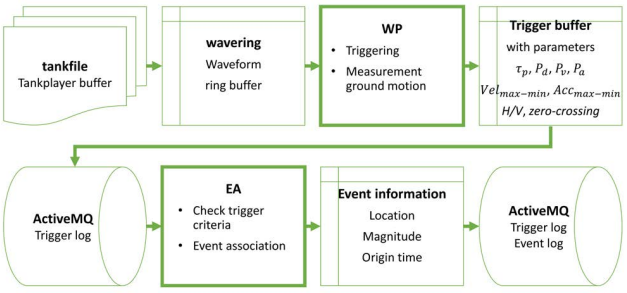

FIGURE 4. Procedure of the EEW simulation system: the difference from a real-time operation is that the start is from a tankfile.

Fig. 4 shows the procedure during the simulation operation. During the simulation, the data read through the tankplayer was transmitted to the wavering player in seconds and temporarily stored. Thereafter, the data stored in the wavering are transmitted to the waveform processor (WP) of ElarmS, and signal detection begins. When a signal was detected through STA/LTA, the module parameters of the initial P-wave, such as P_d, P_v, P_a, and τ_p, were calculated. The detected triggers were stored in ActiveMQ, a data relay server, and transmitted to the event associate (EA) of ElarmS, which calculated the location and magnitude and the association step was performed. Association is a step in collecting triggers identified by the STA/LTA for declaring the occurrence of earthquakes. In this step, the trigger information collected from multiple stations was periodically updated. After calculating the location of the epicenter and magnitude, these values were stored in ActiveMQ.

Additional station and earthquake information updated every second were stored using the previous process. The calculated events were listed by version, and the results were derived. As the version increased, the number of stations used in the association also increased, thereby increasing the accuracy of the analysis. All versions of the event, from the initial version to the end of the calculation, can be recorded on the relay server, and the performance of ElarmS can be confirmed through the information calculated in each version.

V. OPTIMIZING PARAMETERS

In this study, tankfiles of the analyzed 161 earthquakes were generated, and simulations were performed with the module function turned off. As a result, a total of 14,987 P-wave trigger logs were collected from events that were successful in association, and these logs contained the initial P-wave amplitude of the trigger calculated using WP. The collected triggers were analyzed by considering the installation depth of the seismometer. The KMA seismometers were installed at three locations. The first was located on the surface, and a velocity and/or acceleration sensor was used. In most cases, seismometers are installed at positions presumed to be in the bedrock layer. The second was a sensor installed at the

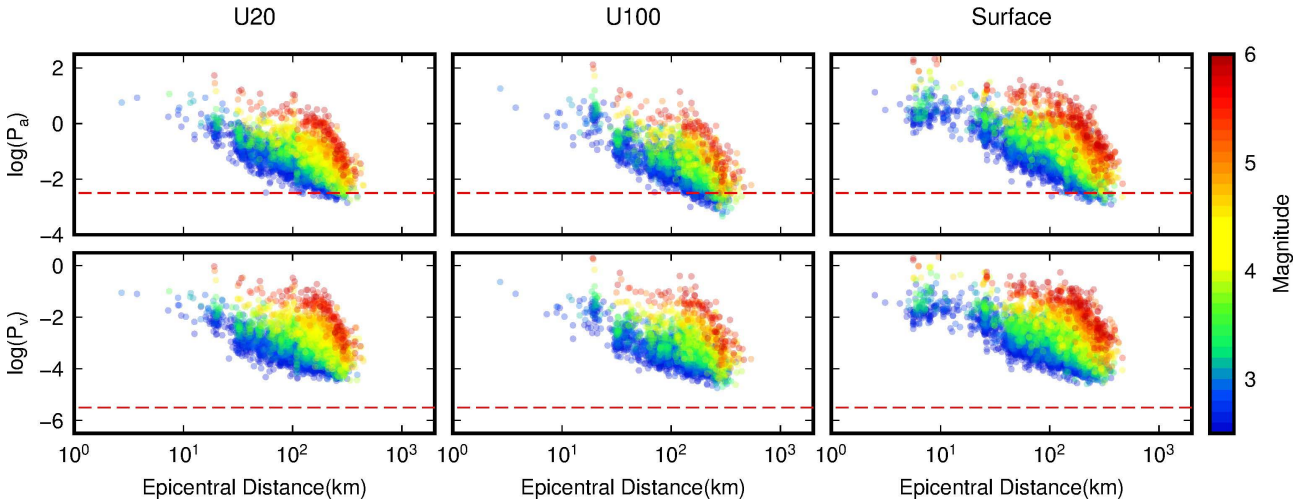

FIGURE 5. Initial P-wave characteristics of the Korean Peninsula; the P-wave amplitude and epicentral distance are expressed as the x- and y-axes, and the gradation color in a circle shows the event magnitude.

bedrock location, called U20. The sensor installed at U20 is an acceleration sensor. Most sensors were installed at a depth of 20 m. If the bedrock was not found before 20 m, the instruments were installed after additional drilling to the bedrock. The third is a velocity sensor installed at the deepest location, underground, and drilled to 100 m. This is called U100.

Fig. 5 illustrates the amplitude characteristics of the initial P-wave according to epicentral distance. At this time, the depth factors cannot be considered because most events on the Korean Peninsula are the intraplate earthquake [25]. The hypocentral depths in event data are dominant within 20 kilometers (Approx 90%). The amplitude of the initial P-wave increased as the magnitude increased. In general, the displacement amplitude of the initial P-wave is highly correlated with the magnitude of the earthquake [18]. Based on Fig. 5, we found that not only displacement, but also velocity and acceleration are highly correlated with the amplitude and magnitude of the P-wave.

The amplitude based on the epicentral distance decreased as the separation distance increased, and the attenuation slope decreased in the order of acceleration and velocity. In the case of the attenuation characteristics, the surface showed a difference between U20 and U100. The amplitude of the initial P-wave recorded underground exhibited linear attenuation characteristics at the log-log scale and nonlinear attenuation characteristics at the surface. The vibration recorded on the surface had a lower attenuation rate in an area with an epicentral distance of 20 km or less than the area with an epicentral distance exceeding 20 km. This is estimated to reflect effects of both the attenuation of vibration transmitted from the shallow soil layer and the effect of the epicentral depth. The red dotted line in Fig. 5 represents the threshold value of the parameter proposed by Chung *et al.* [15]. The records used in this analysis exist on the red dotted line within 250 km. The proposed red dotted line was identified as suitable for earthquake screening. However, the threshold of P_v confirmed that the suggested setting value was excessively conservative. In addition, the threshold of P_a must be adjusted to be slightly lower.

Fig. 6 shows the characteristics of the RPM parameters based on epicentral distance. The attenuation slope and magnitude showed a similar tendency to the previous figure for the initial P-wave amplitude. However, it was found to have relatively high variance. The proposed Chung *et al.* [15] modules were also confirmed to be suitable for screening an earthquake. We confirmed that a threshold adjustment is necessary to set the RPM suitable for seismic data on the Korean Peninsula.

Triggers collected to closely analyze the previously illustrated results were classified based on the depth of installation (surface, U20, and U100) and used for linear regression analysis. Regression analysis was performed in log units to understand the tendency of P-wave amplitude according to epicentral distance, and the basic formula of the regression equation was set as follows:

$$\log(AMP) = a \times \log(R) + b \tag{4}$$

where AMP represents the initial P-wave amplitude (P_v, P_a) or amplitude variation ($\mathrm{Vel_{max}}$-$\mathrm{Vel_{min}}$, $\mathrm{Acc_{max}}$-$\mathrm{Acc_{min}}$), and R is the distance between the source and receiver; a is the attenuation slope, and b is the y-axis intercept that changes depending on the reliability range, which is determined through regression analysis. Table 2 summarizes the log-scaled linear regression values for acceleration. Here, it was organized using a 95% confidence level such that all amplitudes determined based on the epicentral distance could be included without considering the magnitude. The regression analysis for acceleration showed a coefficient of determination of 0.79 to 0.86, and the highest correlation of $r^2 = 0.86$ in the section with a magnitude of 5.0 or higher. The attenuation slope increased as the magnitude increased, whereas the difference in location was not large.

Fig. 7 presents the proposed threshold lines based on parameter analysis. Previously, the attenuation characteristics of the initial P-wave depended on the depth and magnitude

TABLE 2. Log-log scaled linear regression of initial peak acceleration (Pa).

Equation (4)	section	$2.5 \leq M_L < 3.0$	$3.0 \leq M_L < 3.5$	$3.5 \leq M_L < 4.0$	$4.0 \leq M_L < 4.5$	$4.5 \leq M_L < 5.0$	$5.0 \leq M_L$
a	Surface	-1.66	-1.88	-1.96	-2.39	-2.18	-2.40
	U20	-1.59	-1.85	-2.02	-2.24	-2.28	-2.75
	U100	-1.91	-2.15	-2.16	-2.50	-2.63	-2.63
b	Surface	1.29	1.98	2.46	3.61	3.27	4.19
	U20	1.08	1.89	2.50	3.22	3.48	4.92
	U100	1.42	2.20	2.53	3.54	3.89	4.29

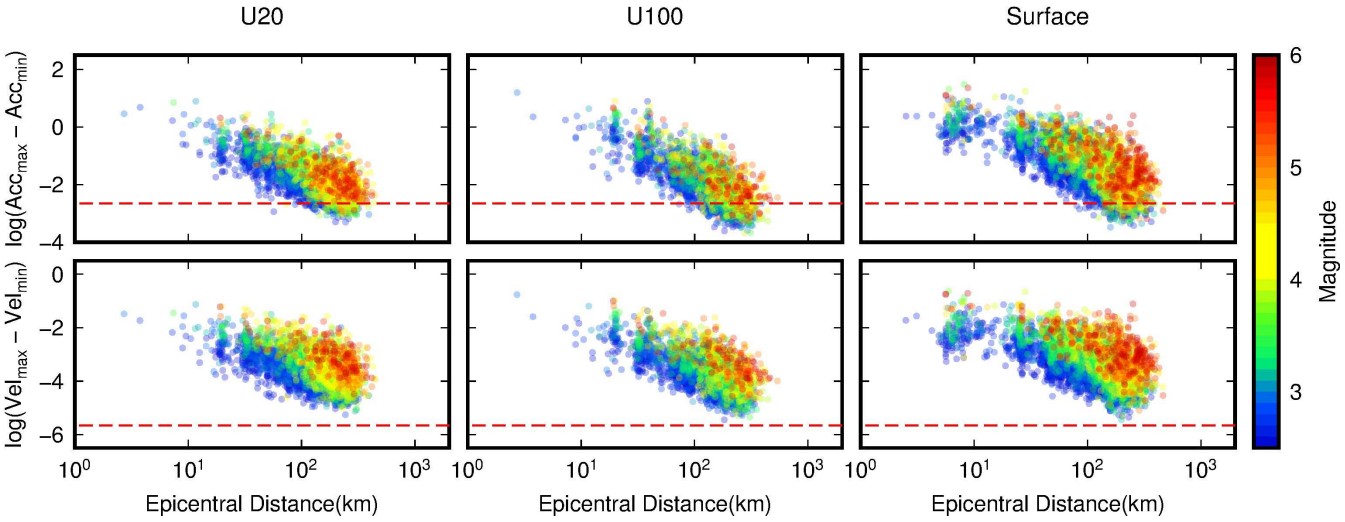

FIGURE 6. Relatively amplitude characteristics of the Korean Peninsula; the wave amplitude and epicentral distance are expressed as the x- and y-axes, and the gradation color in a circle shows the event magnitude.

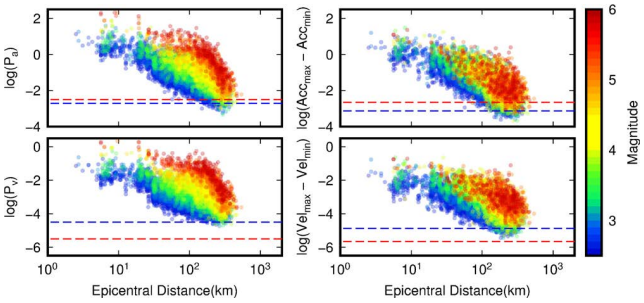

FIGURE 7. Proposal thresholds for a seismic network of the Korean Peninsula: the red line represents the threshold proposed by Chung *et al.* [15], and the blue dotted line represents our proposed threshold.

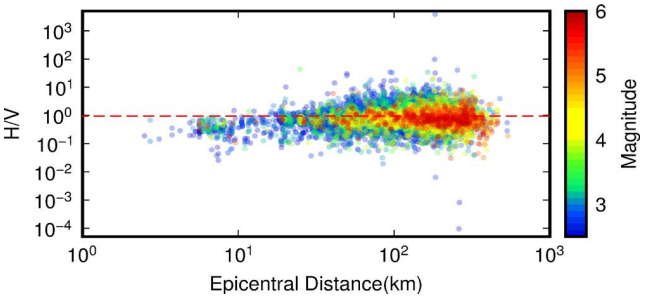

FIGURE 8. Calculated horizontal to vertical component amplitude (H/V) ratio from NEtoZ module: the red line represents the threshold proposed by Chung *et al.* [15].

of the sensor; however, E3 has not yet been applied with an algorithm that considers the installation location of the seismometer. Therefore, we propose a threshold value for the entire signal. The proposed thresholds are values that can sufficiently detect a magnitude of 3.0 or higher within 150 km.

Fig. 8 illustrates the H/V ratio of the NEZM based on epicentral distance. For an earthquake on the Korean Peninsula, the threshold value of the parameter proposed by Chung *et al.* [15] was unsuitable. Based on these results, NEZM was not applicable because of the two characteristics of the observation environment. First, the vertical and horizontal component differences may not be large in the case of the Korean Peninsula, where the frequency of shallow earthquakes is high, and most soil layers are shallow. This is because, based on Snell's law, if the depth of the source is shallow, the incident angle may not be close to the vertical. Second, the amplification effect of the soil layer on earthquake movement is insignificant because the main seismic network of the Korean Peninsula is located in the bedrock below the surface. This suggests that the P- and S-waves cannot be distinguished based on the H/V ratio for earthquakes on the Korean Peninsula.

Based on past earthquake records, the optimal parameters for the Korean Peninsula used in E3 are summarized in

TABLE 3. Optimization criteria based on the historical event.

Module	Parameter	E2	E3 by Chung *et al.* [15]	Proposed thresholds
ACM	τ_p	$-0.9 < \log(\tau_p) < 1.0$	$-0.9 < \log(\tau_p) < 1.0$	$-0.9 < \log(\tau_p) < 1.0$
	P_d	$-5.5 < \log(P_d) < 3.5$	$-5.5 < \log(P_d) < 3.5$	$-5.5 < \log(P_d) < 3.5$
	P_v	-	$-5.5 < \log(P_v) < 3.0$	$-4.5 < \log(P_v) < 3.0$
	P_a	-	$-2.5 < \log(P_a)$	$-2.7 < \log(P_a)$
RPM	Vel_{max} -Vel_{min}	-	Vel_{max} -$Vel_{min} > 2.2\times10^{-6}$cm/s	Vel_{max} -$Vel_{min} > 1.3\times10^{-5}$cm/s
	Acc_{max} -$Accl_{min}$	-	Acc_{max} -$Acc_{min} > 2.2\times10^{-3}$cm/s^2	Acc_{max} -$Acc_{min} > 7.4\times10^{-4}$cm/s^2

TABLE 4. Analysis matrix.

Parameter	*A*	*B*	*C*	*D*	*E*
τ_p	Default	Default	Default	Default	Default
P_d	Default	Default	Default	Default	Default
P_v	Off	Proposed	Off	Off	Proposed
P_a	Off	Off	Proposed	Off	Proposed
Vel_{max} -Vel_{min}	Off	Off	Off	Proposed	Proposed
Acc_{max} -$Accl_{min}$	Off	Off	Off	Proposed	Proposed

TABLE 5. Results of earthquake detection.

	A	*B*	*C*	*D*	*E*
Matched Event	259	264	265	264	268
Missed Event	61	57	56	57	56
False Event	120	111	90	92	82

Table 3. It is difficult to apply different thresholds, depending on the measurement type and installation depth, in the current E3 algorithm. Therefore, the values presented in Table 3 are the minimum threshold values for seismic detection.

VI. VERIFICATION

Simulations were performed using E3 to verify the proposed reference values. To analyze the differences in the optimization, the analysis matrix used in this study is listed in Table 4. Simulations were performed on 329 earthquakes with magnitudes of 2.5, or higher, across the Korean Peninsula from January 1, 2015, to April 30, 2022. *A* was the case where new parameters were not applied and is the same condition as E2; *B*, *C*, and *D* were the cases where new criteria were added; and *E* included all the parameters proposed in this study. Through the five interpretations performed, the effectiveness of the new parameters and the optimization performance were analyzed. All the systems have the same threshold for P_d and τ_p, which is the KMA default. For the reasons mentioned previously, the NEZM and ZCM functions were not used.

The event generation results for each algorithm are summarized in Table 5, and Fig. 9 shows the location of the associated events for algorithms *A* and *E*. Associated events were classified into matched, missed, and false events based on the event origin time and location. A matched event is an earthquake that matches a KMA catalog earthquake within 100 km and 10 s. The match criteria applied a tighter standard in time than the standard proposed by Chung *et al.* [15] to avoid confusion due to sequence earthquakes. A missed event occurs when the system fails to associate events with an earthquake. A false event occurs when the system creates an event, but there is no matching earthquake in the catalog within 100 km and 10 s.

Based on the simulation results, there was no significant difference between the number of matched and missed events for each algorithm. In the case of matched and missed events, most were of low importance as they were earthquakes that occurred in places with poor observatory station coverage and were either small in magnitude or off the observation network.

The number of false events differed for each algorithm. *A* generated 120 false events, which is a significant number compared with the other algorithms. In particular, *C* using the P_a criteria generated fewer false events than *B* using the P_v criteria. These results indicate that the amplitude check in the acceleration unit is effective in improving the performance of the ElarmS. The performance of *D* with RPM is similar to that of *C* because RPM performs amplitude checks on both the velocity and acceleration. When all the parameters were applied simultaneously, the number of false events decreased significantly. Algorithm *E* generated only 82 false events, the smallest among the test algorithms, whereas the number of matched events increased slightly. These results indicate that optimizing the parameters is effective in reducing false alarms and detecting events. The EEW system finally determines whether to produce an alarm by considering the event magnitude, number of stations, station utilization rate, and RMS in the subsequent decision-making step. Hence, the actual number of false alarms may

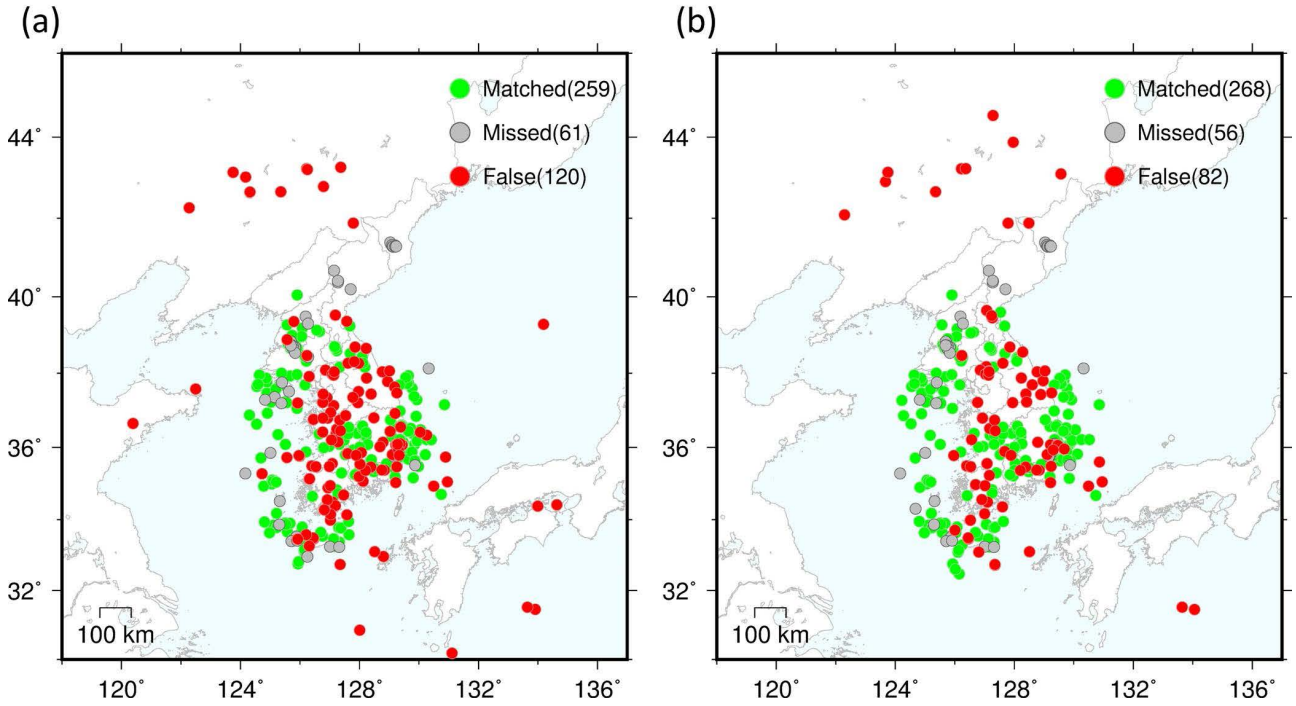

FIGURE 9. Associated event locations for (a) simulation A and (b) E. Green, gray, and red circles indicate matched, missed, and false events respectively.

be less than this result. However, the corresponding results suggest that the optimization of the trigger filter parameters can improve the accuracy and stability of event analysis in the pre-decision-making stage.

VII. CONCLUSION

The empirical P-wave detection technology of ElarmS utilizes an STA/LTA method with a low success rate. Modules that perform quality checks on signals have been added to compensate for this low success rate. In this case, a quality check may be set based on the judgment of an engineer or empirical values. In this study, based on past earthquake records, the vibration characteristics of initial P-waves for earthquakes on the Korean Peninsula were identified, and an optimal threshold was proposed.

An earthquake on the Korean Peninsula is an intraplate earthquake, and the source, path, and site effects are different from those in the western United States, that is, the first development environment of ElarmS. Therefore, parameter analysis is essential for applying the results of the ElarmS to the Korean Peninsula. To this end, we identified new characteristics based on four-year earthquake records.

First, it was confirmed that the attenuation rate of the vertical component of the initial P-wave occurring on the Korean Peninsula varied depending on the magnitude. The attenuation rate was found to increase as the magnitude increased, and the attenuation for acceleration was higher than that for velocity. In addition, attenuation characteristics vary depending on the installation position of the seismometer. In the case of a seismometer located on the surface, attenuation at a location close to the epicenter exhibited nonlinear characteristics, which differed from long-distance attenuation. Based on these characteristics, we found that the installation location of the seismometer must be considered when analyzing earthquakes.

Because the current E3 code cannot consider the positional classification of seismometers, there is no choice but to apply a common threshold value. This is expected to be reflected in the code improvement, and it is necessary to set a threshold based on the classified seismometer. The quality module added to E3 was not applicable to the entire Korean Peninsula. Owing to the nature of the earthquake environment on the Korean Peninsula, it was found that NEtoZ should not be applied. In the case of ZeroCrossing, errors may occur in large earthquakes in certain events; thus, they were excluded.

To verify the parameter optimization, six ElarmS algorithms with different quality modules were constructed, and the simulation results were compared. Based on the results, the added modules sufficiently helped control earthquake signals and contributed to the improvement of the EEW performance. Furthermore, the algorithm to which the new module was applied clearly had a significantly lower occurrence of false events than the previous version.

We proposed a common optimization setting for the KMA's EEW system, which is for Korean networks of seismic stations. However, we found that the amplitude of the initial P-wave depends on the magnitude, epicentral distance, and sensor position of depth. If different thresholds can be applied for each station with an improvement in the algorithm code, it will improve the problem from the STA/LTA trigger.

Unfortunately, we could not propose thresholds for each station in this study because the seismic observation network

on the Korean Peninsula has changed significantly since 2016. Therefore, more event records need to be collected in order for new solutions to be proposed due to the imbalance of each observation. Our analyzes are expected to be referenced in the improvement of the EEW system in the future.

ACKNOWLEDGMENT

The authors thank the associate editor and reviewers for their constructive comments. They also thank Prof. Richard Allen at the University of California at Berkeley for sharing the ElarmS 3.0 algorithm. This study was supported by the Development of Earthquake, Tsunami, Volcano Monitoring, and Prediction Technology.

REFERENCES

[1] R. M. Allen, "Rapid magnitude determination for earthquake early warning," in *The Many Facets Seismic Risk*, vol. 4. Naples, Italy: Università degli Studi di Napoli 'Federico II', 2004, pp. 15–24.

[2] R. M. Allen, "Probabilistic warning times for earthquake ground shaking in the San Francisco bay area," *Seismol. Res. Lett.*, vol. 77, no. 3, pp. 371–376, May 2006, doi: 10.1785/gssrl.77.3.371.

[3] R. M. Allen, "The ElarmS earthquake early warning methodology and application across California," in *Earthquake Early Warning Systems*. Berlin, Germany: Springer, 2007, pp. 21–43.

[4] R. Allen, "Automatic phase pickers: Their present use and future prospects," *Bull. Seismol. Soc. Amer.*, vol. 72, no. 6B, pp. S225–S242, Dec. 1982, doi: 10.1785/bssa07206b0225.

[5] M. Baer and U. Kradolfer, "An automatic phase picker for local and teleseismic events," *Bull. Seismol. Soc. Amer.*, vol. 77, no. 4, pp. 1437–1445, 1987, doi: 10.1785/bssa0770041437.

[6] A. Lomax, C. Satriano, and M. Vassallo, "Automatic picker developments and optimization: FilterPicker—A robust, broadband picker for real-time seismic monitoring and earthquake early warning," *Seismol. Res. Lett.*, vol. 83, no. 3, pp. 531–540, May 2012, doi: 10.1785/gssrl.83.3.531.

[7] Z. E. Ross, M.-A. Meier, E. Hauksson, and T. H. Heaton, "Generalized seismic phase detection with deep learning," *Bull. Seismol. Soc. Amer.*, vol. 108, no. 5A, pp. 2894–2901, 2018, doi: 10.1785/0120180080.

[8] J. Wang, Z. Xiao, C. Liu, D. Zhao, and Z. Yao, "Deep learning for picking seismic arrival times," *J. Geophys. Res., Solid Earth*, vol. 124, no. 7, pp. 6612–6624, 2019, doi: 10.1029/2019jb017536.

[9] L. Zhu, Z. Peng, J. McClellan, C. Li, D. Yao, Z. Li, and L. Fang, "Deep learning for seismic phase detection and picking in the aftershock zone of 2008 M_w7.9 Wenchuan earthquake," *Phys. Earth Planet. Interiors*, vol. 293, Aug. 2019, Art. no. 106261, doi: 10.1016/j.pepi.2019.05.004.

[10] S. M. Mousavi, W. L. Ellsworth, W. Zhu, L. Y. Chuang, and G. C. Beroza, "Earthquake transformer—An attentive deep-learning model for simultaneous earthquake detection and phase picking," *Nature Commun.*, vol. 11, no. 1, p. 3952, 2020, doi: 10.1038/s41467-020-17591-w.

[11] I. Khan and Y.-W. Kwon, "P-detector: Real-time P-wave detection in a seismic waveform recorded on a low-cost MEMS accelerometer using deep learning," *IEEE Geosci. Remote Sens. Lett.*, vol. 19, pp. 1–5, 2022, doi: 10.1109/LGRS.2022.3161017.

[12] M. Zhang, M. Liu, T. Feng, R. Wang, and W. Zhu, "LOC-FLOW: An end-to-end machine learning-based high-precision earthquake location workflow," *Seismol. Res. Lett.*, pp. 1–13, Mar. 2022, doi: 10.1785/0220220019.

[13] A. Datta, D. J. Wu, W. Zhu, M. Cai, and W. L. Ellsworth, "DeepShake: Shaking intensity prediction using deep spatiotemporal RNNs for earthquake early warning," *Seismol. Res. Lett.*, vol. 93, no. 3, pp. 1636–1649, May 2022, doi: 10.1785/0220210141.

[14] H. S. Kuyuk and R. M. Allen, "Optimal seismic network density for earthquake early warning: A case study from California," *Seismol. Res. Lett.*, vol. 84, no. 6, pp. 946–954, Nov. 2013, doi: 10.1785/0220130043.

[15] A. I. Chung, I. Henson, and R. M. Allen, "Optimizing earthquake early warning performance: ElarmS-3," *Seismol. Res. Lett.*, vol. 90, no. 2A, pp. 727–743, 2019, doi: 10.1785/0220180192.

[16] J.-K. Ahn, D. Y. Kwak, and H.-S. Kim, "Estimating VS30 at Korean Peninsular seismic observatory stations using HVSR of event records," *Soil Dyn. Earthq. Eng.*, vol. 146, Jul. 2021, Art. no. 106650, doi: 10.1016/j.soildyn.2021.106650.

[17] A. Oth, M. Böse, F. Wenzel, N. Köhler, and M. Erdik, "Evaluation and optimization of seismic networks and algorithms for earthquake early warning—The case of Istanbul (Turkey)," *J. Geophys. Res.*, vol. 115, no. B10, pp. 1–22, 2010, doi: 10.1029/2010jb007447.

[18] S. Wu, M. Yamada, K. Tamaribuchi, and J. L. Beck, "Multi-events earthquake early warning algorithm using a Bayesian approach," *Geophys. J. Int.*, vol. 200, no. 2, pp. 791–808, Feb. 2015, doi: 10.1093/gji/ggu437.

[19] Y. Wang, S. Li, and J. Song, "Magnitude-scaling relationships based on initial P-wave information in the Xinjiang region, China," *J. Seismol.*, vol. 25, no. 2, pp. 697–710, Apr. 2021, doi: 10.1007/s10950-020-09981-w.

[20] D. Lim, J.-K. Ahn, J. Lee, and D. K. Lee, "Optimization of classification of local, regional, and teleseismic earthquakes in Korean Peninsula using filter bank," *J. Korean Geotech. Soc.*, vol. 35, no. 11, pp. 121–129, 2019.

[21] M. Bracale, S. Colombelli, L. Elia, V. Karakostas, and A. Zollo, "Design, implementation and testing of a network-based earthquake early warning system in Greece," *Frontiers Earth Sci.*, vol. 9, p. 880, Sep. 2021, doi: 10.3389/feart.2021.667160.

[22] D. Sheen, T. Kang, and J. Rhie, "A local magnitude scale for South Korea," *Bull. Seismol. Soc. Amer.*, vol. 108, no. 5A, pp. 2748–2755, Oct. 2018, doi: 10.1785/0120180112.

[23] Y. Wang, S. Li, and J. Song, "Threshold-based evolutionary magnitude estimation for an earthquake early warning system in the Sichuan–Yunnan region, China," *Sci. Rep.*, vol. 10, no. 1, p. 21055, 2020, doi: 10.1038/s41598-020-78046-2.

[24] C. E. Johnson, A. Bittenbinder, B. Bogaert, L. Dietz, and W. Kohler, "Earthworm: A flexible approach to seismic network processing," *IRIS Newslett.*, vol. 14, no. 2, pp. 1–4, 1995.

[25] T.-K. Hong, J. Lee, S. Park, and W. Kim, "Time-advanced occurrence of moderate-size earthquakes in a stable intraplate region after a megathrust earthquake and their seismic properties," *Sci. Rep.*, vol. 8, no. 1, p. 13331, Dec. 2018, doi: 10.1038/s41598-018-31600-5.

SEONGHEUM CHO received the B.S. and M.S. degrees in geophysics from Kangwon National University, South Korea, in 2015 and 2017, respectively. He is currently a Researcher with the Korea Meteorological Administration. His research interests include EEW, ground motion, seismology, seismic tomography, and crustal structure.

JAE-KWANG AHN received the B.S., M.S., and Ph.D. degrees from Hanyang University, South Korea, in 2006, 2008, and 2017, respectively. He is currently a Research Officer with the Korea Meteorological Administration. His research interests include earthquake, ground motion, GANs, EEW, seismic engineering, sensors, liquefaction, and data science.

EUI-HONG HWANG received the B.S., M.S., and Ph.D. degrees from Jeonbuk National University, South Korea, in 1996, 1999, and 2007, respectively. He is currently a Research Officer with the Korea Meteorological Administration. His research interests include earthquake, ground motion, seismology, seismic tomography, and EEW.